Appl Phys A (2011) 104:845–850
DOI 10.1007/s00339-011-6424-y

Applied Physics A
Materials Science & Processing

The effects of thermal annealing on the structure and the electrical transport properties of ultrathin gadolinia-doped ceria films grown by pulsed laser deposition

K. Rodrigo · S. Heiroth · N. Pryds · L. Theil Kuhn · V. Esposito · S. Linderoth · J. Schou · T. Lippert

Received: 6 August 2010 / Accepted: 8 April 2011 / Published online: 11 May 2011

Abstract Ultrathin crystalline films of 10 mol% gadolinia-doped ceria (CGO10) are grown on MgO (100) substrates by pulsed laser deposition at a moderate temperature of 400°C. As-deposited CGO10 layers of approximately 4 nm, 14 nm, and 22 nm thickness consist of fine grains with dimensions $\leq \sim$11 nm. The films show high density within the thickness probed in the X-ray reflectivity experiments. Thermally activated grain growth, density decrease, and film surface roughening, which may result in the formation of incoherent CGO10 islands by dewetting below a critical film thickness, are observed upon heat treatment at 400°C and 800°C. The effect of the grain coarsening on the electrical characteristics of the layers is investigated and discussed in the context of a variation of the number density of grain boundaries. The results are evaluated with regard to the use of ultrathin CGO10 films as seeding templates for the moderate temperature growth of thick solid electrolyte films with improved oxygen transport properties.

K. Rodrigo (✉) · N. Pryds · L. Theil Kuhn · V. Esposito · S. Linderoth
Fuel Cells and Solid State Chemistry Division, Risø DTU, Technical University of Denmark, 4000 Roskilde, Denmark
e-mail: kata@risoe.dtu.dk
Fax: +45-4677-5858

S. Heiroth · T. Lippert
General Energy Research Department, Paul Scherrer Institute, 5232 Villigen PSI, Switzerland

J. Schou
Department of Photonics Engineering, Technical University of Denmark, Risø Campus, 4000 Roskilde, Denmark

1 Introduction

10 mol% gadolina-doped ceria (CGO10) is applied as a key functional component in electroceramic devices, particularly as electrolyte [1–3] in low temperature solid oxide fuel cells (SOFCs) that operate at ∼500°C [4]. Miniaturized SOFCs (μ-SOFCs), currently investigated as promising power sources for portable electronic devices [5–7], require an integration of CGO10 thin film electrolytes into micro-electro-mechanical-systems (MEMS). However, high temperature processing that is conventionally applied in order to acquire high density of thin film electrolytes often leads to film cracking or film delamitation from a substrate, due to the mismatch of the thermal expansion coefficients [8, 9], or to chemical poisoning of the material [10]. This thermally activated degradation of the films can be significantly reduced by thin film preparation via pulsed laser deposition (PLD) as its inherent nonequilibrium growth conditions [11] enable the growth of dense crystalline CGO10 films at comparatively low temperatures [8, 9]. However, the resulting films are often characterized by a high density of nm-sized growing nuclei [12]. The connected high number density of grain boundaries causes a grain boundary-limited, degraded ionic conduction of the films [12, 13] due to the resistive nature of the internal interfaces. Multi-step growth involving the preparation of ultrathin seed layers in the first stage to control the growth and physical properties of the subsequent (thick) coating [14, 15] is envisioned as an option to overcome these limitations, enabling the deposition of coarse grained CGO10 films at moderate temperatures, which is advantageous for solid electrolyte applications.

This work reports on the effects of different thermal annealing treatments on the morphology, microstructure, and electrical transport properties of ultrathin CGO10 layers with thicknesses in the range of 4–25 nm. We have explored

Table 1 Annealing conditions for the CGO10 seed layers

Annealing temperature	Dwell time
as-deposited	–
400°C	1 h
800°C	1 h
	10 h

the preparation conditions for suitable seed templates. The CGO10 films are prepared on MgO (100) substrates in order to enable their electrical characterization. The films are studied by atomic and lateral force microscopy, X-ray reflectivity, and d.c. resistivity measurements.

2 Experimental procedure

CGO10 films with thicknesses of 4.4 ± 0.2 nm, 13.7 ± 1.1 nm, and 22.2 ± 1.4 nm were grown on MgO (100) substrates by pulsed laser deposition in a high vacuum chamber [16]. A rotating sintered CGO10 target was ablated by a KrF excimer laser beam (λ: 248 nm, τ: 20 ns, f: 10 Hz) focused to a spot size of 3.6 mm^2 yielding a fluence of 1.1 J/cm^2. The ablated material was deposited at normal incidence on a substrate mounted to a rotary sample holder positioned in a distance of 68 mm to the target. All depositions were conducted at a fixed substrate temperature of 400°C in an oxygen background atmosphere with a pressure of 1.0 Pa. The ultrathin seed layers were exposed to different post-annealing treatments (Table 1) under an oxygen flux of 20 sccm in a tubular furnace applying a heating and cooling rate of 3 K/min.

Specular X-ray reflectometry (XRR) measurements of the layers were acquired in a 2θ-range of 0.25–7° at an incremental step width of 0.02° and an integration time of 15 s/step on a Siemens D500 diffractometer applying Cu K_α radiation. The presence of a magnesium hydroxide layer at the substrate surface, which forms readily upon exposure to humid air, was taken into account within the simulation of the experimental XRR patterns using the GenX software [17] that yielded information on the thickness, roughness, and density of the CGO10 layers.

The topographical surface roughness and morphology were analyzed by atomic force microscopy (AFM) using a Nanoscope IIIa scanning probe microscope (Digital Instruments/Veeco Inc.) in a contact mode. The average lateral grain size was estimated by Heyn's mean lineal intercept method [18], measuring at least 500 individual grains. Operation in lateral force microscopy (LFM) mode was applied to monitor surface friction contrast.

The "in-plane" electrical characterization of the 13.7 ± 1.1 nm and 22.4 ± 1.4 nm thick layers was performed by continuous two-point d.c. conductivity measurements using a Keithley 2700 multimeter. The measurements were conducted in air at a flow rate of 10 sccm, utilizing a heating and cooling rate of 2 K/min, on samples with sputter-deposited, 2 mm spaced silver electrodes of about 400 nm thickness, which were connected with Ag paste and Pt wires. Multiple heating and cooling cycles were applied, in order to validate the stability of the electrical response.

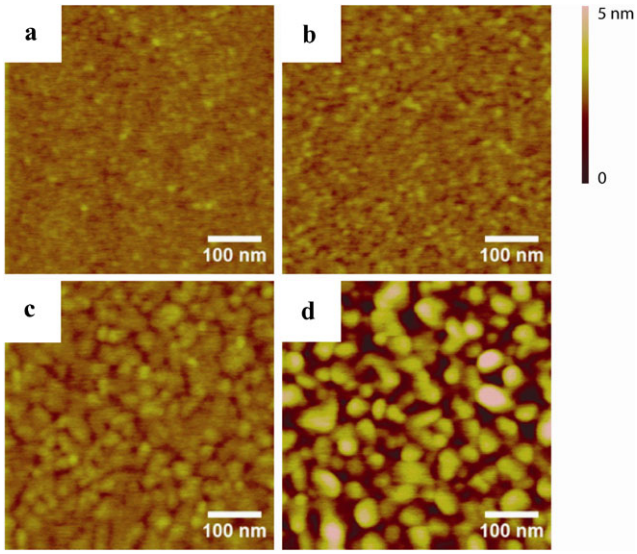

Fig. 1 Topographical AFM images of 22.2 ± 1.4 nm thick CGO layers grown on MgO(100) substrates by PLD and subsequently exposed to different heat treatments: as-deposited (**a**), annealed at 400°C for 1 h (**b**), annealed at 800°C for 1 h (**c**) and annealed at 800°C for 10 h (**d**)

3 Results and discussion

The topography of the as-deposited and heat-treated CGO10 layers is depicted representatively for the set of 22.2 ± 1.4 nm thick films in Fig. 1. The AFM images clearly show a change of the layer morphology induced by the thermal treatment. The feature size increases and the formation of distinct grains is promoted by the heat treatment (Fig. 1b–d) compared to the as-deposited state (Fig. 1a). The quantitative results of the thermally activated grain growth are summarized in Table 2. The as-deposited layers exhibit fine grains with dimensions $\leq \sim$11 nm, close to the lower limit for a reliable size estimation. Annealing at 400°C for 1 h results only in minor grain coarsening. However, a significant increase of the mean lateral grain size (D) by a factor of 2.3–3.5, proceeding with progressing exposure time on an hour time scale, is observed if the annealing temperature is elevated to 800°C. As Table 2 reveals, D increases moreover systematically with the film thickness, which accounts for the coarsening of the growing nuclei with progressing material deposition during PLD.

In addition to the thermally activated grain growth, the annealing affects the surface roughness (R) of the coatings. The drop of the interference fringe amplitude in the XRR patterns (Fig. 2) points qualitatively to an increase of the film roughness with increasing annealing time and temperature. Table 2 compares the quantitative roughness data obtained by the AFM and an analysis of the XRR patterns and consistently confirms this trend with a particularly pronounced increase of R in the case of prolonged (10 h) exposure at high temperature (800°C). However, the roughness of surfaces measured by the AFM is systematically smaller than that obtained by the XRR technique. This variation might be resulting from the difference in the nature of the XRR and the AFM measurements. In contrast to the AFM, where film topography is directly measured, the XRR probes the electron density normal to the substrate surface. This implies sensitivity to the chemical composition of the layer. Hence, the systematically higher XRR roughness values compared to the purely topographical AFM reference data suggest a chemical roughness component, i.e., the presence of a compositional gradient at the film surface. Although the impurity [19] or dopant [20] segregation to interfaces is well known, this effect is not expected in films prepared at low deposition temperature of 400°C [21]. Thus, an additional factor, like a convolution of the film topography and the tip shape and size [22] that might lead to contradicting trends in the AFM roughness measurements, has to be also taken into consideration in order to explain the differences in roughness obtained by the two methods.

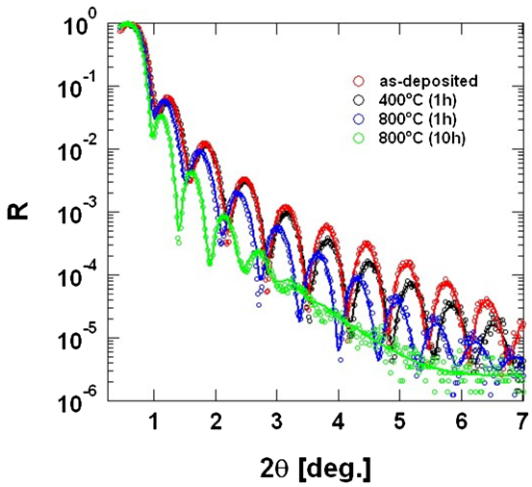

Fig. 2 Specular X-ray reflectivity patterns of 13.7 ± 1.1 nm thick CGO10 layers exposed to different post-annealing treatments. The *solid lines* represent least square simulations with a two layer model $MgO/MgO{\cdot}(H_2O)_x/Ce_{0.9}Gd_{0.1}O_{1.95}$ by the GenX software

Below a critical thickness the surface roughening can ultimately lead to the disintegration of the continuous CGO10 films and the formation of isolated islands. This is observed for the 4.4 ± 0.2 nm thick CGO10 layer annealed at 800°C for 10 h, as seen in Fig. 3. Distinct, about 27 ± 3 nm wide features form upon the heat treatment from an originally smooth and uniform film as indicated by the topographical AFM image (Fig. 3a). The friction contrast, manifested by the mirror-like appearance of the LFM images in a trace and re-trace direction (see Fig. 3b and c), unambiguously proves the presence of two chemically different phases, assigned to the MgO substrate surface and isolated CGO10 islands. The observed dewetting behavior shows that homo-binding forces are stronger than hetero-binding forces in the CGO10/MgO system.

Table 2 Average grain size (D), topographical rms roughness (R_q), XRR surface roughness (R), and film density (ρ), as a function of the thickness (t), and heat treatment of the CGO10 seed layers

t [nm]	Annealing	D [nm]	R_q (AFM) [Å]	R (XRR) [Å]	ρ [g/cm^3]
4.4 ± 0.2	as-deposited	<10	1.3 ± 0.1	1.8 ± 0.1	7.24 ± 0.10
	400°C (1 h)	<10	1.1 ± 0.1	2.9 ± 0.1	7.08 ± 0.12
	800°C (1 h)	24.3 ± 0.7	2.1 ± 0.2	3.5 ± 0.1	7.05 ± 0.03
	800°C (10 h)	27 ± 3	–*	–*	–*
13.7 ± 1.1	as-deposited	10.8 ± 0.4	1.3 ± 0.1	2.3 ± 0.2	7.15 ± 0.06
	400°C (1 h)	13.3 ± 0.5	1.6 ± 0.1	3.3 ± 0.2	7.21 ± 0.05
	800°C (1 h)	25.1 ± 0.8	2.2 ± 0.3	4.5 ± 0.3	6.92 ± 0.05
	800°C (10 h)	35.7 ± 1.3	8.2 ± 0.7	11.0 ± 0.8	7.02 ± 0.12
22.2 ± 1.4	as-deposited	11.3 ± 0.5	2.1 ± 0.1	2.4 ± 0.3	7.14 ± 0.14
	400°C (1 h)	19.0 ± 0.7	2.3 ± 0.1	3.6 ± 0.3	7.03 ± 0.08
	800°C (1 h)	27.6 ± 0.9	2.7 ± 0.4	4.9 ± 0.2	6.89 ± 0.02
	800°C (10 h)	39.1 ± 1.3	9.8 ± 0.4	14.4 ± 1.8	6.92 ± 0.15

*Not estimated due to the CGO10 layer discontinuity

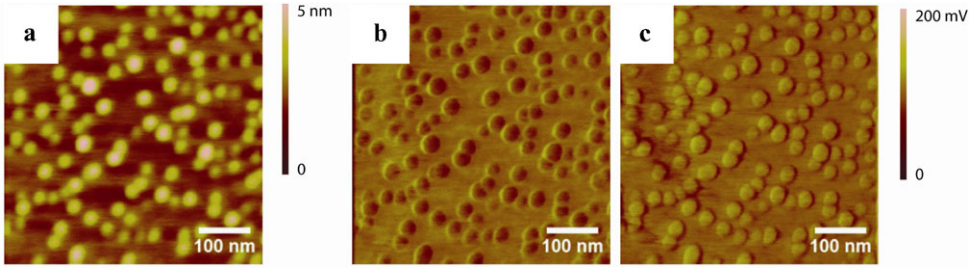

Fig. 3 Topographical AFM image (**a**) and lateral force microscopy (LFM) images in the trace (**b**) and retrace direction (**c**) obtained after annealing of a 4.4 ± 0.2 nm thick CGO10 seed layer grown on MgO(100) at 800°C for 10 h

In addition to the dampening of the interference fringe amplitude the XRR patterns in Fig. 2 reveal a shift of the critical angle below the reference value of 0.362 deg (dispersion correction not included in the estimation) for the fully dense CGO10 material. Accordingly, the deduced density (ρ) of the layers decreases with the intensity of the heat-treatment (compare Table 2). Generally, the densities of the as-deposited layers and those annealed for 1 h at 400°C are close (99–98%) to the theoretical density of CGO10, i.e., 7.226 g/cm^3 assuming nominal oxygen stoichiometry given by the doping level. This proves that the layers are without significant internal pores within the probed thickness, i.e., 7.4 nm at the critical angle. The apparent density drop down to 95–97% observed for the layers heat treated at 800°C is counter-intuitive since higher annealing temperatures commonly cause a densification. Most probably this effect is an artifact from the surface roughening that lowers the integrated effective density and does not relate to changes of the films crystallographic density or the formation of internal porosity.

The compilation of the total electrical conductivity (σ) at 600°C, 700°C, and 800°C, as well as the values of the activation energy (E_a) are presented in Fig. 4 for the sets of 13.7 ± 1.1 nm and 22.2 ± 1.4 nm thick CGO10 layers. The thinnest layers (4.4 ± 0.2 nm average thickness) were excluded from the electrical measurements, as the applied measurement geometry did not yield measurable resistances.

In Fig. 4a–b, the electrical properties of the layers with an average thickness of 13.7 ± 1.1 nm (solid symbols) and 22.2 ± 1.4 nm (open symbols) are presented as a function of the grain size, whereas in Fig. 4c–d these properties are depicted as a function of the thickness of the individual layers. As a general trend, an increase of the grain size results in an increase of the conductivity (see Fig. 4a). Moreover, one can notice that the conductivity of films with similar grain sizes and varying thickness differs. The thinner layers (13.7 ± 1.1 nm) are less conductive, i.e., the conductivity equals on average 0.0019 ± 0.0006 S/cm, 0.007 ± 0.002 S/cm, and 0.027 ± 0.004 S/cm at 600°C, 700°C, and 800°C, respectively. The thicker films (22.2 ± 1.4 nm) are characterized by slightly higher conductivity values, i.e., 0.0037 ± 0.001 S/cm, 0.014 ± 0.003 S/cm, and 0.038 ± 0.007 S/cm at 600°C, 700°C, and 800°C, respectively. A closer inspection of the grain size and the film thickness dependence of E_a (see Fig. 4b and 4d) gives additional insight into the electrical properties of the films. The decrease of E_a (from 1.40 ± 0.02 eV to 1.10 ± 0.02 eV) with increasing grain size (see Fig. 4b-solid points) and increasing thickness (see Fig. 4 d-solid points) follows the increase of the conductivity (see Fig. 4a and Fig. 4c-solid points). A stable E_a value of 1.00 ± 0.01 eV, independent of the grain size, is approached for films with a thickness ≥ ∼20 nm. Only the CGO10 layer of the largest investigated thickness and grain size reveals deviation from the mentioned trends and the rest of the data, i.e., systematically lower conductivities and an activation energy of 1.10 ± 0.02 eV. This might be related to a contamination or a poor contact quality of that particular sample.

The absolute conductivity values for the ultra-thin, nano-grained films are low compared to a bulk microcrystalline CGO10, which exhibits, e.g., a total conductivity of 0.018 S/cm at 600°C combined with a lower activation energy for the total conduction of $E_a = 0.83$ eV [12]. Figure 4 suggests that the films electrical conductivity improves with the presence of larger grains formed either by prolonged PLD growth (thicker films) or subsequent thermal annealing. This can be rationalized in terms of the lower number density of grain boundaries that possess a high specific resistance to the transport of oxygen ions, which has been attributed to the formation of vacancy-depleted space charge regions [23]. These results are in contrast to some reports [24] claiming an enhancement of the electrical transport properties in nanocrystalline ion conductors.

These results suggests that thermal annealing could be used to prepare suitable, coarse grained seeding templates for the moderate temperature growth of CGO10 electrolyte films that provide enhanced ionic transport properties compared to a single step, direct deposition. Nevertheless, prolonged exposure to relatively high annealing temperatures (800°C) is required to induce significant grain coarsening. A seed layer thickness above 5 nm is recommended to avoid

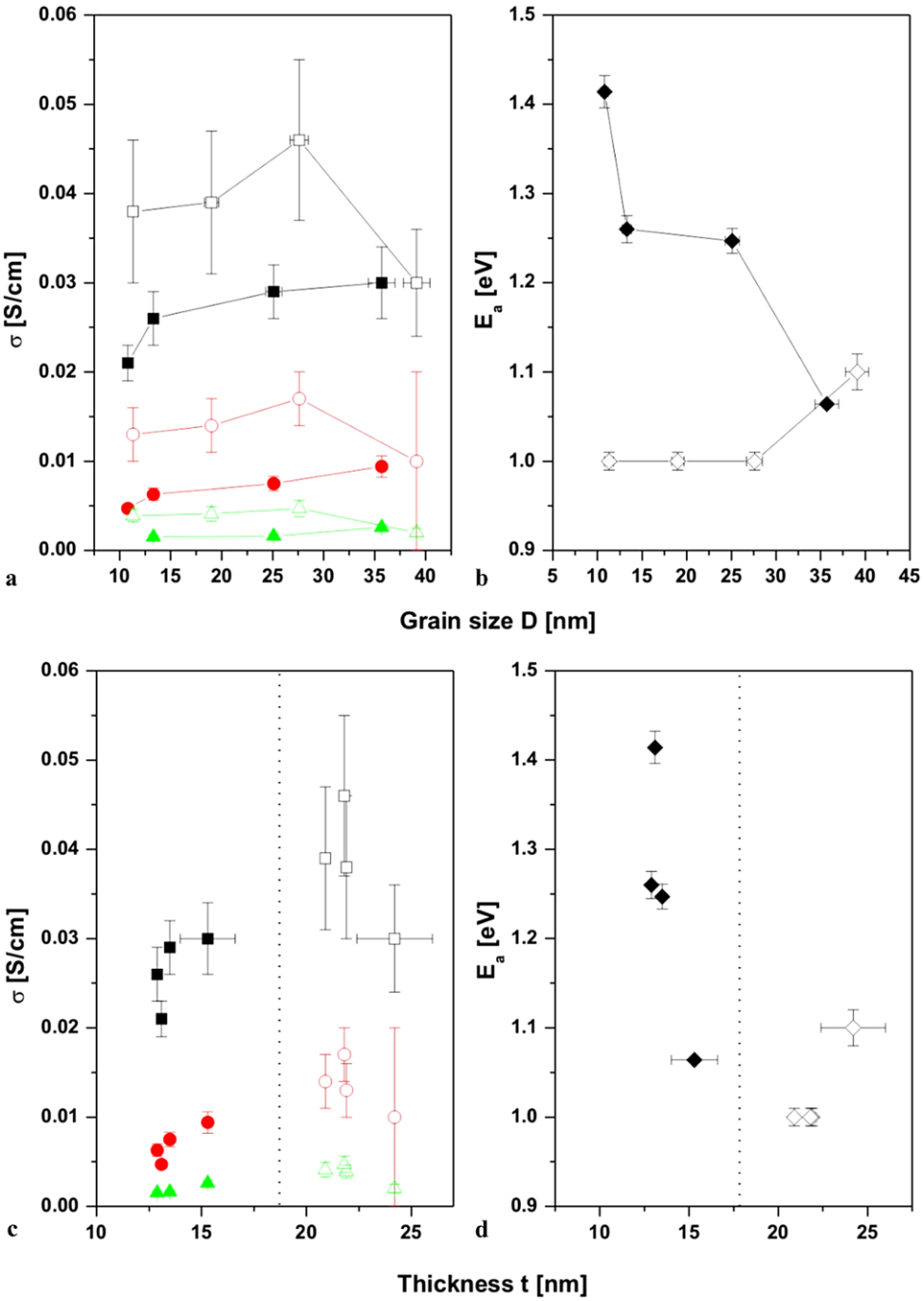

Fig. 4 Total conductivity as a function of grain sizes for the 13.7 ± 1.1 nm (*closed symbols*) and 22.2 ± 1.4 nm (*open symbols*) thin CGO10 films (**a**). The *triangles*, *circles* and *squares* correspond to data obtained at 600°C, 700°C, and 800°C, respectively. Activation energy as a function of the average grain size (**b**). Total conductivity of the layers as a function of the layer thickness for both sets of samples (**c**). Activation energy as a function of the layer thickness (**d**). The *error bars* are based on the experimental errors in the determination of the film thickness and grain size

disintegration of the films by dewetting under the required harsh annealing conditions.

4 Conclusions

Ultrathin (thickness: 4–25 nm) polycrystalline CGO10 layers are grown by PLD at a moderate temperature of 400°C. The density of the as-deposited films reaches 98–99%, as established within the applicability limits of the XRR method. The as-deposited layers consist of nm-sized grains with dimensions below 10 nm. Prolonged exposure to high annealing temperatures (800°C) is necessary to induce significant grain growth resulting, e.g., in average grain sizes of 35–40 nm after 10 h. Simultaneously, the surface roughness increases, which may ultimately result in a disintegration of the originally continuous film into isolated islands below a critical layer thickness of 5–10 nm. The electrical conductivity increases with the grain size and film thickness while the activation energy decreases to values ∼1.0 eV. These

changes are due to the reduction of the number density of blocking grain boundaries. The experimental results suggest that only high temperature thermal annealing is an eligible option to prepare coarse grained ultrathin CGO10 layers as suitable seeding templates for the moderate temperature growth of solid electrolyte thin films with enhanced ionic transport properties compared to the direct single step deposition.

Acknowledgements The authors would like to acknowledge Dr. K.M. Kant, Mr. F. Saxild, Mr. J. Geyti for technical assistance in PLD depositions.

References

1. J.A. Kilner, Solid State Ion. **129**, 13 (2000)
2. M. Mogensen, N.M. Sammes, G.A. Tompsett, Solid State Ion. **129**, 63 (2000)
3. B.C.H. Steele, Solid State Ion. **129**, 95 (2000)
4. R.T. Leah, N.P. Brandon, P. Aguiar, J. Power Sources **145**, 336 (2005)
5. H. Huang, M. Nakamura, P. Su, R. Fasching, Y. Saito, F.B. Prinz, J. Electrochem. Soc. **154**, B20 (2007)
6. S. Rey-Mermet, P. Muralt, Mater. Res. Soc. Symp. Proc. **972**, 0972-AA07-10-BB08 (2007)
7. A. Bieberle-Hütter, D. Beckel, A. Infortuna, U.P. Muecke, J.L.M. Rupp, L.J. Gauckler, S. Rey-Mermet, P. Muralt, N.R. Bieri, N. Hotz, M.J. Stutz, D. Poulikakos, P. Heeb, P. Müller, A. Bernard, R. Gmür, T. Hocker, J. Power Sources **177**, 123 (2008)
8. K. Rodrigo, S. Heiroth, M. Döbeli, N. Pryds, S. Linderoth, J. Schou, T. Lippert, J. Optoelectron. Adv. Mater. **12**, 511 (2010)
9. A. Infortuna, A. Harvey, L. Gauckler, Adv. Funct. Mater. **18**, 127 (2008)
10. R. Gerhardt, A.S. Nowick, J. Am. Ceram. Soc. **69**, 647 (1986)
11. P.R. Willmott, Progr. Surf. Sci. **76**, 163 (2004)
12. K. Rodrigo, S. Heiroth, M. Lundberg, N. Bonanos, K. Mohan Kant, N. Pryds, L. Theil Kuhn, V. Esposito, S. Linderoth, J. Schou, T. Lippert, Appl. Phys. A **101**, 601 (2010)
13. X. Guo, E. Vasco, S. Mi, K. Szot, E. Waschsman, R. Waser, Acta Mater. **53**, 5161 (2005)
14. C.-Y. Zhang, X.-M. Ki, X. Zhang, W.-D. Yu, J.-L. Zhao, J. Cryst. Growth **290**, 67 (2006)
15. T. Chaudhuri, P. Spagnol, S. Phok, R. Bhattacharya, Physica C **443**, 81 (2006)
16. N. Pryds, B. Toftmann, J.B. Bilde-Sørensen, J. Schou, S. Linderoth, Appl. Surf. Sci. **252**, 4882 (2006)
17. M. Björck, G. Andersson, J. Appl. Crystallogr. **40**, 1174 (2007)
18. G.F. Vander Voort, F.J. Warmuth, S.M. Purdy, A. Szirmae (eds.), *Metallography—Past, Present, and Future 75th Anniversary Volume* (American Society for Testing and Materials, Philadelphia, 1993)
19. K.V. Hansen, K. Norrman, M. Mogensen, Surf. Interface Anal. **38**, 911 (2006)
20. Y.M. Chiang, E.B. Lavik, D.A. Blom, Nanostruct. Mater. **9**, 633 (1997)
21. K. Rodrigo, H.-J. Wang, S. Heiroth, N. Pryds, L. Theil Kuhn, V. Esposito, S. Linderoth, J. Schou, T. Lippert, Appl. Surf. Sci. **257**, 5341 (2011)
22. D.L. Sedin, K.L. Rowen, Appl. Surf. Sci. **182**, 40 (2001)
23. J. Maier, Solid State Ion. **157**, 327 (2003)
24. I. Kosacki, T. Suzuki, V. Petrovsky, H.U. Anderson, Solid State Ion. **136–137**, 1225 (2000)